6
The production of polarized hadrons

Crucial to all the preceding chapters is the assumption that we are able to produce beams and targets of polarized particles and that we are able to analyse the state of polarization of these particles.

In the production of targets and beams we are dealing with stable particles (or at least particles stable on the time scale involved) and the physics involved is basically a mixture of classical and quantum mechanics.

There has been extraordinary progress in the design and construction of polarized proton sources at Argonne and Brookhaven and in the development of highly polarized, radiation-resistant targets of various materials by workers at CERN, Fermilab, HERA, Basel, Virginia, SLAC and Ann Arbor.

Great advances have been made in the resolution of problems involved in the acceleration of polarized protons by groups at Bloomington and at Brookhaven. The electron beams at LEP and at HERA have been successfully polarized and a superb polarized electron source is in use at SLAC.

Also quite remarkable has been the building of secondary and tertiary beams of polarized hyperons at Fermilab. Who would have believed it possible that one can measure the magnetic moment of the Ω^-?!

Firstly we shall provide a brief discussion of the physical principles of polarized proton sources and targets and of the problems involved in accelerating beams of polarized protons without loss of polarization.

We also discuss a relatively new development, the attempt to polarize protons and antiprotons via the Stern–Gerlach effect.

Finally we consider the construction and functioning of the secondary and tertiary hyperon beams at Fermilab.

In Chapter 7 we shall study electron sources and the beautiful phenomenon whereby electron beams in a circular accelerator acquire a natural polarization (which in a perfect machine is $\approx 92\%$!) as a consequence

https://doi.org/10.1017/9781009402040.006 Published online by Cambridge University Press

of synchroton radiation. Polarimetry, the measurement of polarization, is taken up in Chapter 8.

The 'real-life' physics of sources, accelerators and targets is, of course, highly technical, even, to some extent, an 'art', so of necessity our treatment will emphasize only the main physical principles. For further information and access to the literature consult the series of proceedings of the International Symposium on High Energy Spin Physics (ISHESP, 1996).

6.1 Polarized proton sources

All polarized proton sources have as their aim the production of a beam of polarized ions ready for acceleration. There are many types and the produced ions may be positively or negatively charged. We shall discuss only the production of a beam of polarized protons in an atomic-beam type of source.

To understand the physics one must bear in mind the following.

(i) The S-wave ground state of the hydrogen atom is split by the hyperfine interaction into eigenstates $|s\,m\rangle$ of total spin: the spin singlet

$$|0;0\rangle = \tfrac{1}{\sqrt{2}}\{|\uparrow_e\downarrow_p\rangle - |\downarrow_e\uparrow_p\rangle\} \tag{6.1.1}$$

and the spin triplet

$$\begin{gathered} |1;1\rangle = |\uparrow_e\uparrow_p\rangle \qquad |1;-1\rangle = |\downarrow_e\downarrow_p\rangle \\ |1;0\rangle = \tfrac{1}{\sqrt{2}}\{|\uparrow_e\downarrow_p\rangle + |\downarrow_e\uparrow_p\rangle\} \end{gathered} \tag{6.1.2}$$

where the arrows indicate the spin projections of electron and proton.

(ii) The triplet-state energy is

$$\Delta \approx 6 \times 10^{-6}\ \text{eV} \tag{6.1.3}$$

above the singlet.

(iii) By comparison, the spin–orbit splitting is orders of magnitude greater ($\approx$ eV).

(iv) The interaction with an external magnetic field B is largely controlled by the electron, since for the magnitude of the magnetic moments

$$\mu_e \sim 660\mu_p \approx 5.8 \times 10^{-5}\ \text{eV/T}. \tag{6.1.4}$$

(v) Boltzmann's constant is

$$k \approx 0.86 \times 10^{-4}\ \text{eV/K}. \tag{6.1.5}$$

https://doi.org/10.1017/9781009402040.006 Published online by Cambridge University Press

As a consequence, for a hydrogen atom in a field B there is a transition region around $B \approx 0.1$ T below which the hyperfine interaction dominates and above which the interaction between the electron and the external field takes over. The energy levels are shown in Fig. 6.1 as a function of B in tesla.

The labelling of the states $|a\rangle$, $|b\rangle$, $|c\rangle$, $|d\rangle$ has become conventional. One has

$$\begin{aligned} |b\rangle &= |\downarrow_e\downarrow_p\rangle \qquad |d\rangle = |\uparrow_e\uparrow_p\rangle \\ |a\rangle &= \cos\theta\ |\downarrow_e\uparrow_p\rangle - \sin\theta\ |\uparrow_e\downarrow_p\rangle \\ |c\rangle &= \sin\theta\ |\downarrow_e\uparrow_p\rangle + \cos\theta\ |\uparrow_e\downarrow_p\rangle \end{aligned} \tag{6.1.6}$$

where $\tan 2\theta \approx \Delta/(2\mu_e B)$.

Note that for strong fields

$$|a\rangle \to |\downarrow_e\uparrow_p\rangle$$

and

$$|c\rangle \to |\uparrow_e\downarrow_p\rangle.$$

An example of a polarized proton source is shown in Fig. 6.2. A beam of thermal hydrogen molecules passes through an intense rf field, which dissociates the molecules into hydrogen atoms. At the temperatures involved, the hydrogen atoms populate all the hyperfine states equally, so the beam is essentially unpolarized; it is then passed through a strong

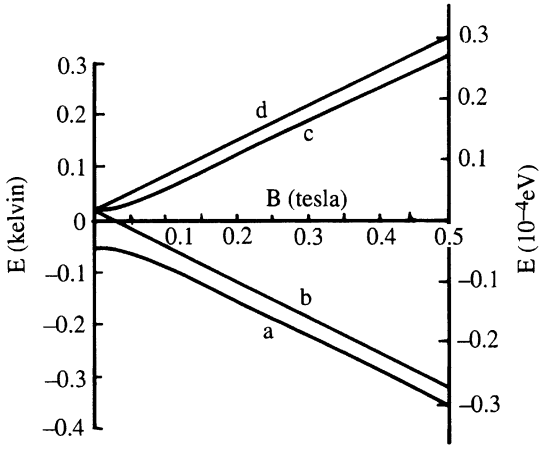

Fig. 6.1 Lowest energy levels of a hydrogen atom in a magnetic field B. $B = 0$ corresponds to the hyperfine splitting.

https://doi.org/10.1017/9781009402040.006 Published online by Cambridge University Press

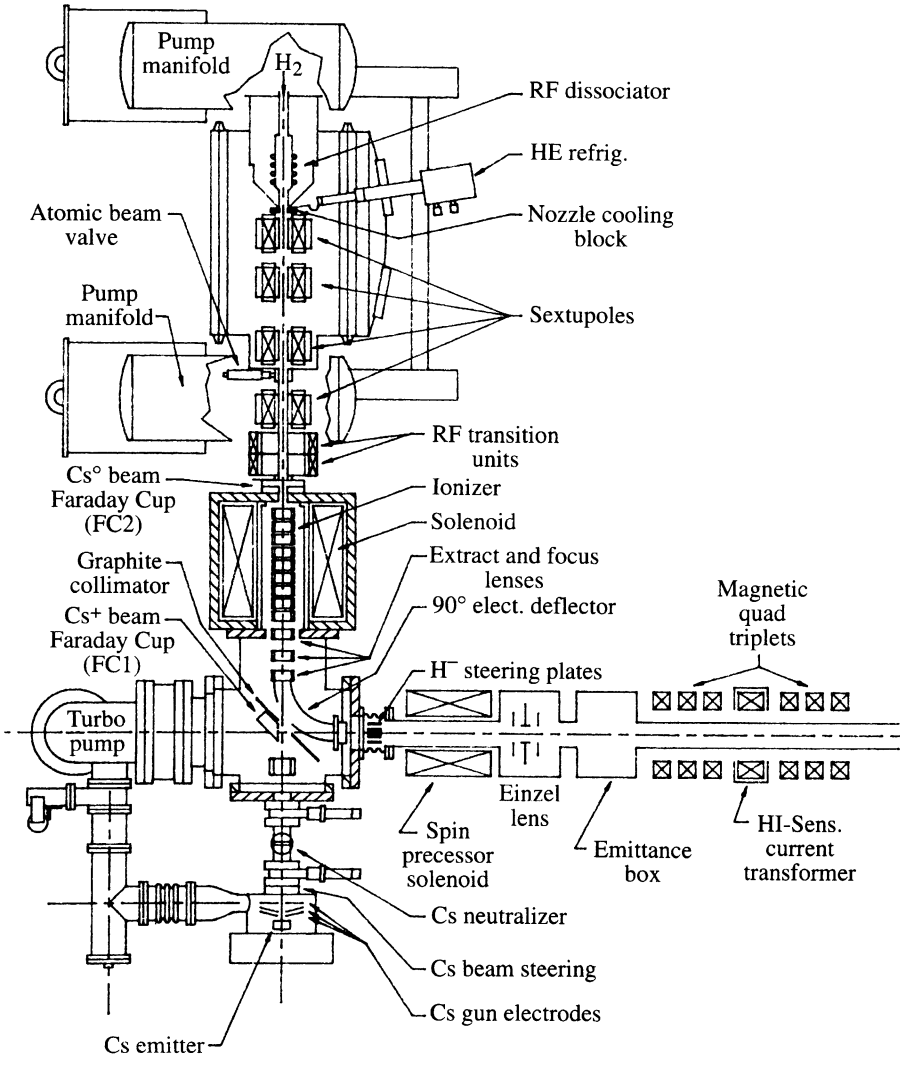

Fig. 6.2 Schematic diagram of the Brookhaven AGS polarized beam source (courtesy of Y. Makdisi).

sextupole magnet. The inhomogeneous field acts as a Stern–Gerlach apparatus separating the atoms in the states $|\uparrow_e\uparrow_p\rangle$ and $|\uparrow_e\downarrow_p\rangle$ from those in the states $|\downarrow_e\downarrow_p\rangle$ and $|\downarrow_e\uparrow_p\rangle$. The point of using a sextupole to provide the inhomogeneous field is that it *focusses* the atoms in the one pair of states while *defocussing* the others. Thus the beam that emerges contains the states $|\uparrow_e\uparrow_p\rangle$ and $|\uparrow_e\downarrow_p\rangle$ i.e. the *electron* spin, is totally polarized. The beam then passes through a uniform magnetic field and an rf field

https://doi.org/10.1017/9781009402040.006 Published online by Cambridge University Press

that induces transitions from $|\uparrow_e\downarrow_p\rangle$ to $|\downarrow_e\uparrow_p\rangle$. The electrons are thereby depolarized but the protons are now completely polarized in the state $\uparrow_p$. The atoms pass through an ionizing field that strips off the electrons and one is left with a beam of polarized protons.

The angle of the mean spin relative to the direction of motion can be altered by using the fact that, at *non-relativistic* energies, when a proton is deflected by an electric field the mean spin essentially does not change direction. This is most easily seen from the discussion of the dynamics of the relativistic mean spin vector given in subsection 6.3.1 below, in particular from eqn (6.3.22). In this way one finally obtains a source of polarized protons whose mean spin vector is perpendicular to the plane of the accelerator into which the beam is fed.

The most ambitious series of spin measurements ever undertaken has just begun at the RHIC accelerator at Brookhaven, where proton–proton collisions up to a CM energy of 500 GeV will be possible, with both beams polarized and with a high luminosity $\mathscr{L} = 2 \times 10^{32}\ \text{cm}^{-2}\ \text{s}^{-1}$. To achieve this, use is made of a new source which yields 500 μA of current.

6.2 Polarized proton targets

Two developments seem to offer the most promise for high energy physics: (1) the construction of targets using frozen ammonia, and (2) the use of gas jets or cells of polarized protons. We shall briefly discuss their essential features.

6.2.1 Frozen targets

In many polarization experiments one requires a high-intensity beam. This causes problems in the target for two reasons. It creates a heat load that requires a high-powered cryogenic system and it causes radiation damage to the material, resulting in a fall-off in polarization. Ammonia is found to be more resistant to radiation damage than other target materials and its ability to become polarized can be recovered by a process of annealing. In addition the fraction of the target material that becomes polarized is higher ($\approx 18\%$) than in other materials.

Consider a diamagnetic solid into which are embedded some paramagnetic impurities, which, for our purposes, can be considered as localized electron spins. The embedding can be done by chemical doping or by irradiation in an electron beam.

For temperatures of the order of 0.5 K and for magnetic fields of the order of 2.5 T the electron spins will be almost completely aligned whereas the protons spins will be unpolarized. The polarization of the electrons

https://doi.org/10.1017/9781009402040.006 Published online by Cambridge University Press

is transferred to the protons via a process known as 'dynamical nuclear polarization'.

Let us suppose that all electron spins are in the thermal equilibrium state $\uparrow_e$ and that there is a dipole–dipole coupling between the electron spins and the neighbouring proton spins. Under a microwave field of the correct frequency, transitions $|\uparrow_e\downarrow_p\rangle \rightarrow |\downarrow_e\uparrow_p\rangle$ can be induced while $|\uparrow_e\uparrow_p\rangle \not\rightarrow |\downarrow_e\downarrow_p\rangle$. Of course the reverse transition $|\downarrow_e\uparrow_p\rangle \rightarrow |\uparrow_e\downarrow_p\rangle$ also takes place, so that there would be no change in the proton polarization if the only mechanism were the electron spin resonance effect. But the electron spins, via coupling to the lattice, have a relaxation time that is orders of magnitude shorter than that of the proton spins, so that the flipped electron spin $\downarrow_e$ rapidly returns to its thermal equilibrium state $\uparrow_e$, from which it can once again induce a proton spin-flip $\downarrow_p \rightarrow \uparrow_p$. In this fashion the electron spin polarization is transferred to the proton spins.

With this method, polarizations of about 70% could be reached in two hours and the target could handle beams of about 10^{10} protons per second. A major improvement was achieved at Ann Arbor when Crabb *et al.* (1990), working at 1 K and using a 5 T field, succeeded in obtaining a polarization of 96% in about 25 minutes! To what extent such polarizations can be achieved in a beam depends critically on the power of the cooling system.

The above frozen ammonia target has been further developed by a Virginia, Basel, SLAC group (Crabb and Day, 1995) and used very successfully in the polarized electron beam at SLAC in the E143 experiment. Using a ^{4}He evaporation refrigerator with a large pumping system, it was operated at temperatures ≤ 1 K in a beam of 5×10^{11} electrons per second while retaining substantial polarization.

Experiments were done using normal ammonia, $^{14}NH_3$, and deuterated ammonia, $^{14}ND_3$, as well as with $^{15}NH_3$ and $^{15}ND_3$, since in the isotope ^{15}N the unpaired polarizable neutron in ^{14}N is paired with a second neutron. This leads to smaller corrections when trying to interpret a measured asymmetry as a proton asymmetry. Proton polarizations of about 80% and deuteron polarizations of about 40% were achieved under actual experimental running conditions.

Figures 6.3 and 6.4 give some idea of the complexity of an ethylene glycol target and a frozen ammonia target. For a review of solid polarized targets, see Crabb and Meyer (1997).

One of the most influential experiments of the 1980s was the European Muon Collaboration (EMC) measurement of deep inelastic lepton–proton scattering. This used longitudinally polarized muons incident upon a

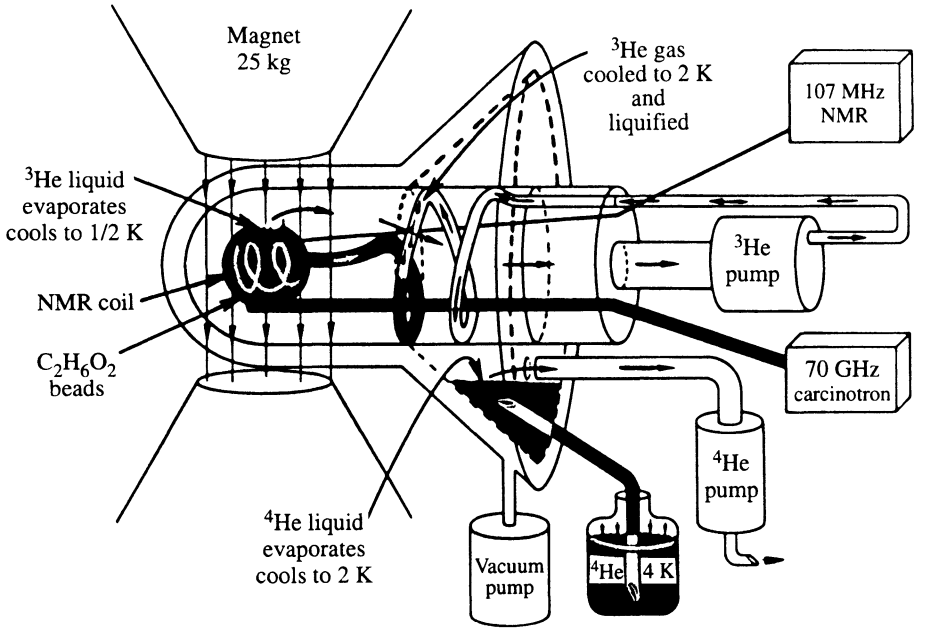

Fig. 6.3 Ethylene glycol target using ^{3}He evaporation cryostat (courtesy of A.D. Krisch).

longitudinally polarized proton target (Ashman *et al.*, 1988). The startling results of this collaboration, which are discussed in Section 11.5, stimulated enormous theoretical and experimental interest and their work has been continued by the Spin Muon Collaboration (SMC) at CERN. Building upon the experience of the EMC, the apparatus and especially the targets used by the SMC reached a remarkable level of refinement. For proton data a frozen ammonia target was used and for deuteron data the target material was deuterated butanol. The target material was contained in two identical thin cylindrical cells, one behind the other, with the beam traversing them longitudinally, as shown in Fig. 6.5. The material in the upstream and downstream cells had opposite polarizations – of great help in eliminating systematic errors.

A typical polarization build-up induced by the microwave field takes several hours, but to obtain maximum polarization takes several days. When the microwave power is switched off the target is operated in the 'frozen-spin' mode at extremely low temperatures, of 30–50 mK. This is only possible because of the relatively low intensity of the muon beam, about 2×10^7 per second.

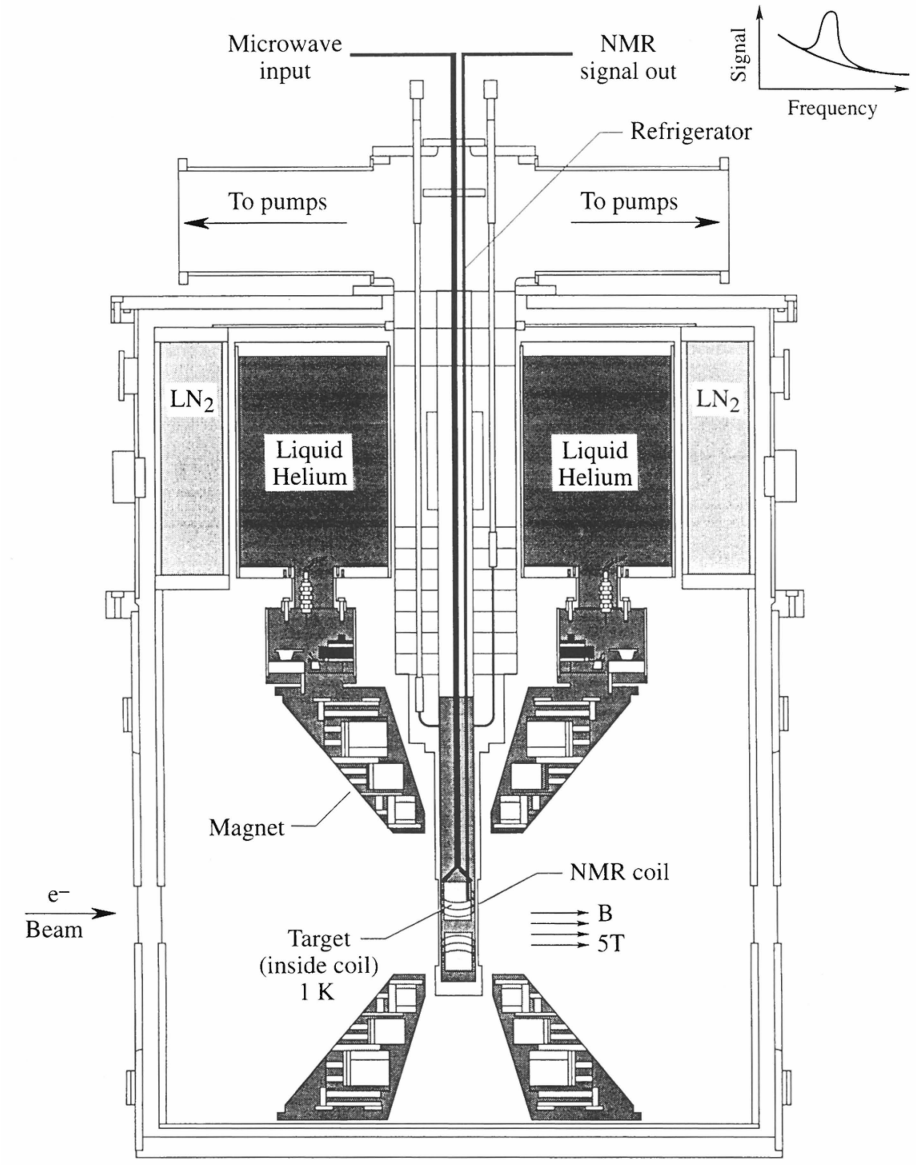

Fig. 6.4 Virginia, Basel, SLAC frozen ammonia target using ^{4}He refrigerator (courtesy of D.G. Crabb).

Once in a frozen-spin mode the direction of the longitudinal polarization can be reversed relatively quickly by varying the fields in the various magnets that surround the target. Typically the polarization was reversed five times per day. It was also possible to rotate the direction of polarization into a direction transverse to the beam.

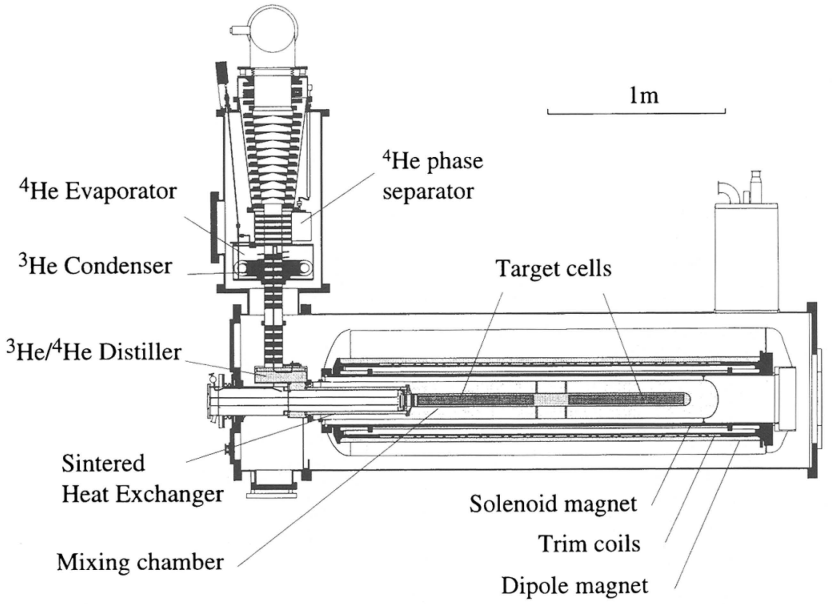

Fig. 6.5 Polarized target used by the Spin Muon Collaboration at CERN. On the left, the dilution refrigerator; on the right the target cells within a system of superconducting magnets. (Courtesy of G. Mallot.)

The average polarizations achieved and the accuracy to which they were known are impressive:

$$\langle \mathscr{P}_p \rangle = 0.86 \pm 0.02 \qquad \langle \mathscr{P}_d \rangle = 0.50 \pm 0.02.$$

6.2.2 *Gas-jet targets*

Unpolarized gas jets have been used for some time in hadronic physics. The jet is fired across the circulating beam in the accelerator and the low density of the jet compared with a solid target is compensated by the large number of times the beam bunch traverses the jet. The construction of a *polarized* jet has been discussed for a long time (Dick *et al.*, 1980). A great advantage over the solid polarized targets discussed in subsection 6.2.1 is that in an atomic hydrogen jet all the material of the jet is polarized, not just a small fraction of it.

We shall discuss three types of polarized-gas-jet target:

(i) the Mark-II ultra-cold polarized-hydrogen-jet target being developed at Ann Arbor for use as an internal target to study proton–proton collisions at the 400 GeV UNK proton accelerator under construction at Protvino;

https://doi.org/10.1017/9781009402040.006 Published online by Cambridge University Press

(ii) the HERMES polarized-proton gas cell already in use at HERA in measurements of deep inelastic electron–proton scattering; and
(iii) the SLAC high-density gaseous polarized ^{3}He target in use at SLC for electron–^{3}He scattering, which yields very direct information on electron–neutron scattering.

(*i*) *The Mark II ultra-cold polarized-hydrogen-jet target*

The basic idea, which was suggested many years ago (Niinikoski, 1980; Kleppner and Greytak, 1982) seems at last to be on the point of becoming a practical tool; see Fig. 6.6(a). The aim is to have a low-velocity jet of intensity of about 4×10^{17} atoms per second, giving an equivalent target thickness of 10^{13} polarized protons per cm^2, a figure more than an order of magnitude better than achieved with conventional atomic beam sources (for a status report see Luppov *et al.*, 1996).

One of the challenging problems is to avoid spoiling the very high vacuum (10^{-9} torr) required in the regime of the jet. Thus the vertical jet must be captured very efficiently after the jet passes across the accelerator beam. For this purpose a so-called 'cryocondensation catcher' pump has been developed with an extremely high pumping speed, for atomic hydrogen, of about 1.2×10^7 litres per second!

The basic idea is to accumulate electron-polarized atomic hydrogen in a magnetic storage bottle at densities greater than 10^{18} atoms/cm^3 and then produce the beam by electron spin resonance microwave pumping. The crucial point is that unpolarized hydrogen atoms at the above density will rapidly combine to form molecular hydrogen, whereas atoms whose electron spins are parallel experience a weak repulsion.

Hydrogen atoms are produced in an rf dissociator and then rapidly cooled to ≈ 0.3 K. They flow into a cell lying inside a 12 T superconducting solenoid. The nature of the cell walls is critical since atomic hydrogen is absorbed strongly on most surfaces. To avoid this, the surfaces are coated with liquid ^{4}He. For such high fields the spin states given in eqn (6.1.6) become

$$\begin{aligned} |b\rangle &= |\downarrow_e\downarrow_p\rangle \qquad & |a\rangle &= |\downarrow_e\uparrow_p\rangle \\ |d\rangle &= |\uparrow_e\uparrow_p\rangle \qquad & |c\rangle &= |\uparrow_e\downarrow_p\rangle \end{aligned} \tag{6.2.1}$$

and atoms in states $|a\rangle$ and $|b\rangle$ are accelerated by the field gradient towards the high-field region and escape from the cell. The atoms in states $|c\rangle$ and $|d\rangle$ are repelled towards the low-field region and effuse from the exit aperture with the electron spin polarized. (Other forces are, of course, totally dominated by the magnetic moment of the electrons.)

The beam then passes through an rf transition unit (see Fig. 6.6(a)), where microwaves are injected at a suitable frequency to induce, say, the transition $|c\rangle \rightarrow |a\rangle$. The resulting beam with all protons polarized in the

state $\uparrow_p$ passes through a superconducting sextupole magnet that focusses the atoms in state $|a\rangle$ into the interaction region while defocussing the atoms in state $|d\rangle$; the latter are cryopumped away.

Recently it has been discovered that a quasi-parabolic copper mirror, coated with superfluid ^{4}He, gives enhanced focussing of the emerging beam and might lead to an order-of-magnitude increase in the beam intensity (Fig. 6.6(b)).

This whole development is extremely attractive and could lead to jets with essentially 100% polarization and with sufficient density to be able to study large-momentum-transfer reactions, where severe tests of QCD may be possible (see Chapters 12 and 13).

(ii) The HERMES polarized-gas cell

This is not strictly a gas-jet target, in the sense that instead of simply crossing the circulating electron beam the gas flows through a T-shaped open ended pipe or storage cell, as shown in Fig. 6.7, so that the gas forms a longitudinal tube along the direction of the electron beam. The incoming gas jet is produced in conventional fashion from an atomic-beam source, as described in Section 6.1, and without the longitudinal cell would produce an effective target thickness of a few times 10^{11} protons per cm^2. With the cell, effective thicknesses of about 10^{14} protons per cm^2 have been achieved. On the negative side, the cell walls present a source of background scattering (which in a proton beam might present a severe problem) and it is necessary to collimate the electron beam so as to prevent the tail of the beam from scattering off the cell walls.

The HERMES source was first tested in 1994 using unpolarized gas. During 1995 it ran with polarized ^{3}He with stable polarizations of about 50% and in 1996 functioned successfully with hydrogen and deuterium, achieving proton polarizations of 80%–90%. The quality and stability of the ^{3}He polarization is vividly illustrated in Fig. 6.8.

The principle used to produce polarized ^{3}He in the HERMES experiment will be explained briefly. (A somewhat more detailed explanation of the SLAC ^{3}He target is given in the next subsection.) The method was first exploited by Colegrove, Schearer and Walters (1963) and the more modern variant now utilized is described in Lee *et al.* (1993). Helium-3, with a nuclear spin of 1/2, possesses a 1^1S_0 ground state and a 2^3S_1 metastable excited state, which is easily excited by a weak electrical discharge. Placed in a weak magnetic field these levels undergo a hyperfine splitting. If, using a tunable laser, the gas is now optically pumped with, say, left-circularly-polarized light propagating in the direction of the magnetic field, transitions can be excited out of the $J_z = -3/2$ and $-1/2$

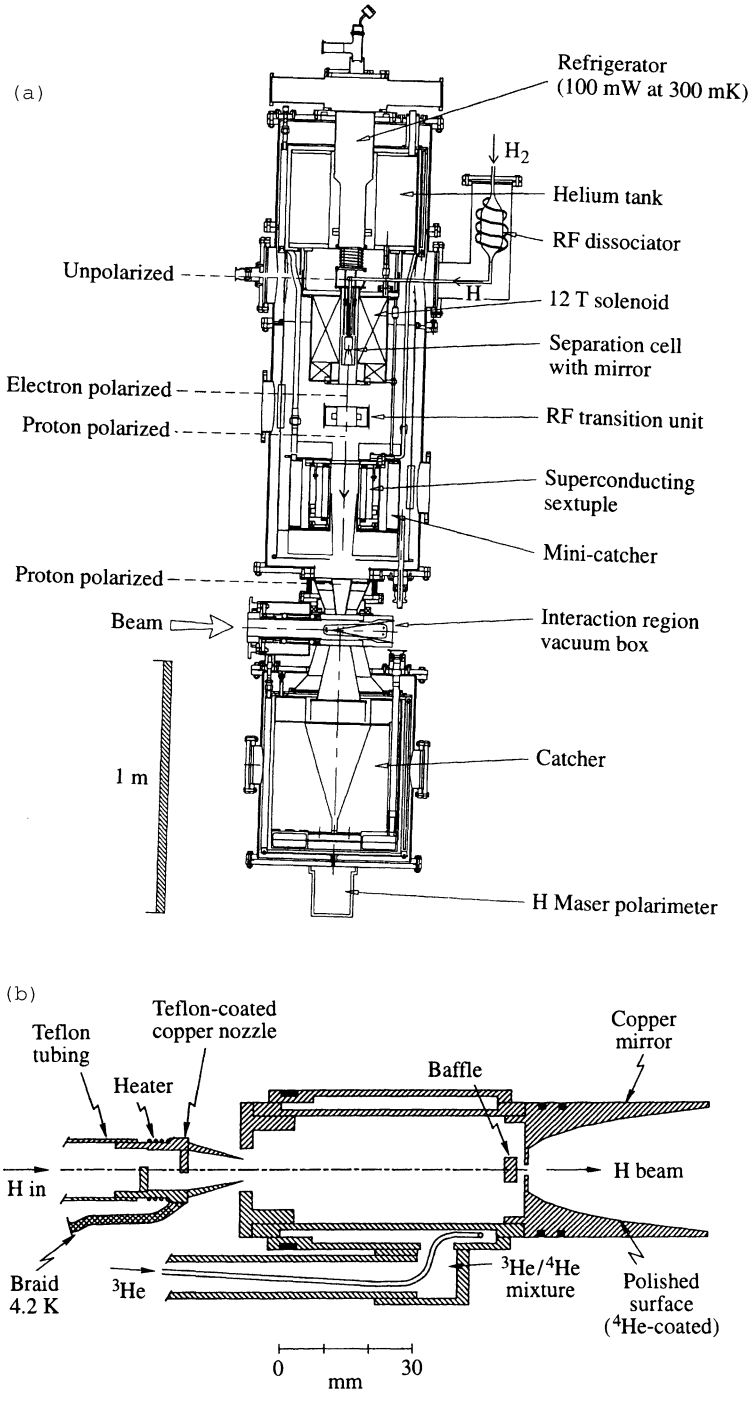

Fig. 6.6 (a) Mark-II ultra-cold polarized-hydrogen-jet target (courtesy of A. D. Krisch); (b) mechanism for improved focussing.

https://doi.org/10.1017/9781009402040.006 Published online by Cambridge University Press

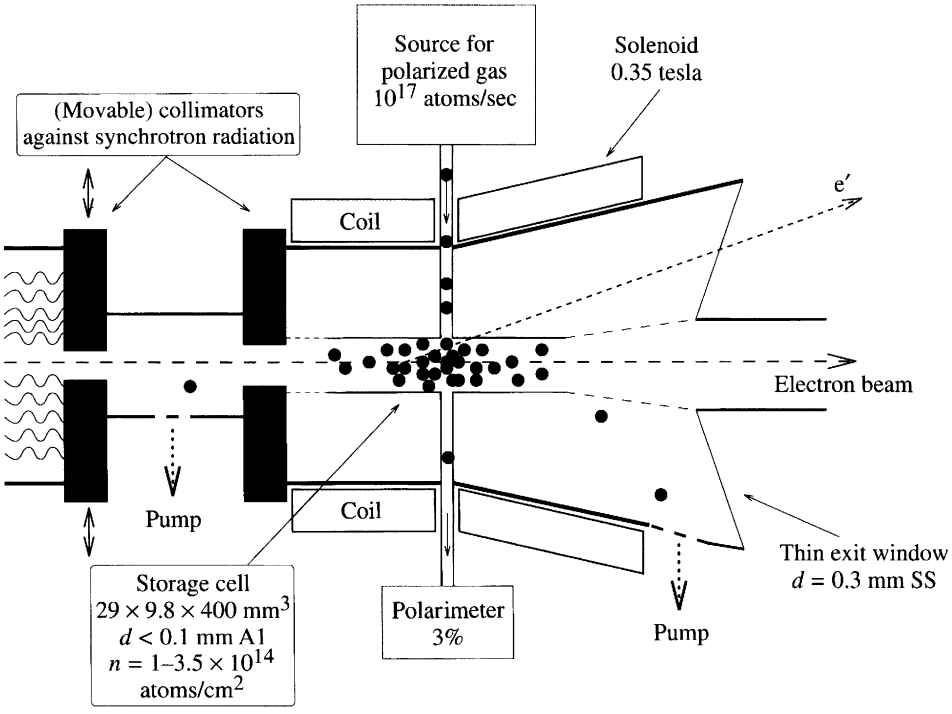

Fig. 6.7 Schematic view of the HERMES polarized gas cell (courtesy of W. Lorenzon).

hyperfine sub-levels of the $^3S_1$ state to certain of the $^3P_0$ sub-levels. Collision mixing then populates all the $^3P_0$ sub-levels and these decay back to the $^3S_1$ sub-levels with equal probability. There is thus a net depletion of the metastable $J_z = -3/2$ and $-1/2$ sub-levels. In collisions between the polarized metastable atoms and atoms in either sub-level of the ground state there is some probability of a transfer of angular momentum, leading to the polarization of the ground state atoms, i.e. to the polarization of the ^{3}He nuclei, since the electrons in the ground state are in a $^1S_0$ state.

(iii) The SLAC high-density gaseous polarized ^{3}He *target*

Polarized ^{3}He is an ideal target for studying electron–neutron interactions because, it is believed, the nucleus is essentially in a spatially symmetric S-state where the spins of the two protons must be in opposite directions. Thus the spin of the nucleus is almost entirely provided by the neutron and only very small corrections are required to extract the 'true' polarized neutron results from the ^{3}He results.

The idea of a ^{3}He target is not new (Bouchiat *et al.*, 1960), but a high-density target capable of operating effectively in the presence of an

https://doi.org/10.1017/9781009402040.006 Published online by Cambridge University Press

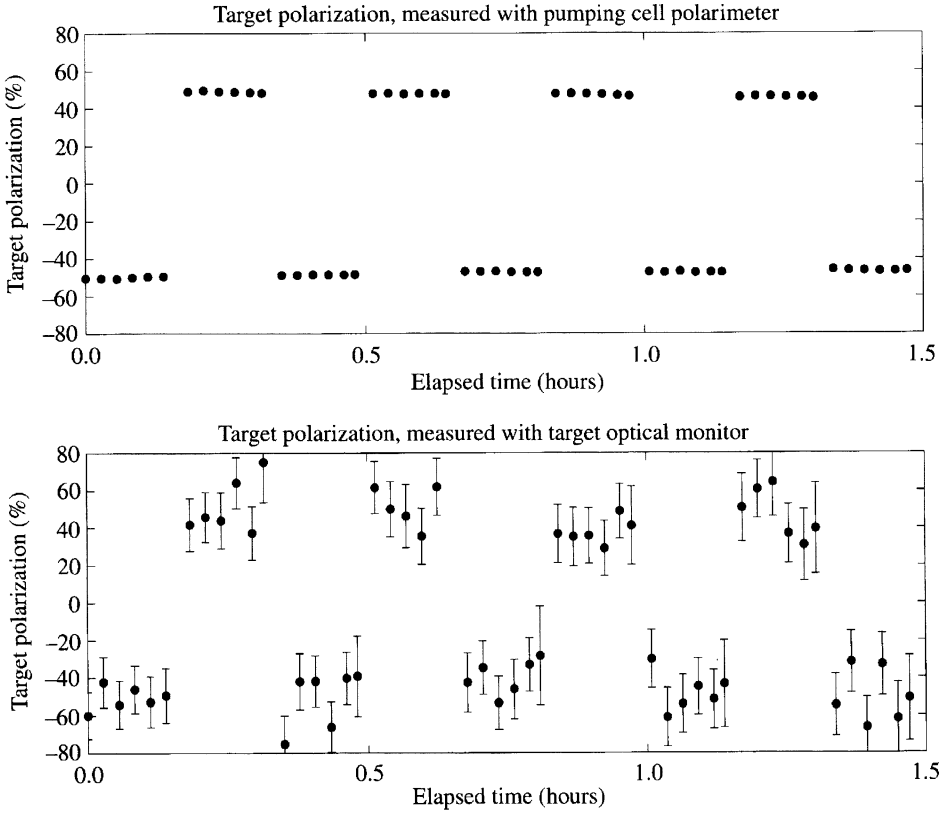

Fig. 6.8 Polarization of ^{3}He in the HERMES gas cell as a function of time, measured by two methods (courtesy of W. Lorenzon).

intense electron beam is a non-trivial matter and a prototype of the SLAC target was first developed in 1992 by a Harvard–MIT team (Chupp *et al.*, 1992).

The essential physical mechanism involved in the polarizing of the ^{3}He is reasonably straightforward and is based on spin transfer in collisions between ^{3}He and highly polarized Rb. Rubidium ($Z = 37$), an alkali metal, has one valence electron outside a closed shell, so that in the ground state it is in a $5S_{1/2}$ state. The Rb vapour lies in a uniform static magnetic field $\mathbf{B}_0$, which defines the Z-direction, and is optically pumped using circularly polarized (σ^+) light of wavelength 794.7 nm from a Ti: sapphire laser, with the beam directed along $\mathbf{B}_0$. In this process the electron, in the ground state with $J_z = -1/2$ is excited to the $^5P_{1/2}$ state, with $J_z = 1/2$. The low-density Rb vapour, with about 10^{14} atoms/cm^3, is immersed in ^{3}He gas of a much higher density ($> 10^{20}$ atoms/cm^3) so that as a result of the high collision rate and the very small energy differences between

https://doi.org/10.1017/9781009402040.006 Published online by Cambridge University Press

the various P states, the Rb P-states become equally populated and the radiative decay back to the ground state feeds the $J_z = \pm 1/2$ states with equal probability. There is thus a net depletion of the ground state with $J_z = -1/2$ until eventually the Rb vapour becomes electron-spin-polarized along $\mathbf{B}_0$, in the ground state $J_z = 1/2$, at which point it is transparent to the σ^+ light.

In the collisions between the Rb and the ^{3}He, a very tiny part of the interaction is due to a hyperfine interaction between the Rb valence electron and the ^{3}He nucleus and thus leads to an extremely small, but non-zero, probability for spin exchange. Provided that mechanisms for depolarization are weak enough, there will then be a slow transfer of the valence-electron polarization to the ^{3}He nucleus.

Herein lies the technical challenge. The polarization build-up time is very long, about 10 hours! So one has to construct a target in which the many potential sources of depolarization (or spin relaxation) are minimized to a fantastic degree. Foremost amongst these dangers are:

(a) in an intense electron beam the rubidium will be depolarized through ionization;
(b) radiation damage will darken the glass cell walls and prevent optical repumping of the cell.

The two-cell structure shown in Fig. 6.9 was a brilliant solution to these problems (Chupp *et al.*, 1992; Johnson *et al.*, 1995). The upper cell, lying in an oven, contains the Rb vapour and the ^{3}He and is connected via a transfer tube to the sealed target cell, which lies in the electron beam. The ^{3}He is polarized in the upper cell and diffuses through to the target cell with a time constant of about 10 minutes (much smaller than the characteristic times for spin relaxation). The target cell remains at a much lower temperature than the upper cell so that the Rb vapour density therein is negligible. The actual physical construction of such a two-chamber cell is incredibly difficult and it is a triumph that it has been possible to produce targets with effective densities of about 7×10^{21} ^{3}He nuclei per cm^2 with a stable polarization of 40% over periods of several weeks!

6.3 The acceleration of polarized particles

We discuss here the problems that arise when one tries to accelerate polarized particles, namely, the mechanisms that tend to depolarize the particles and how these can be overcome. The motion of a particle in an accelerator is largely a question of classical dynamics and the behaviour of the spin is best understood in terms of the covariant mean spin vector

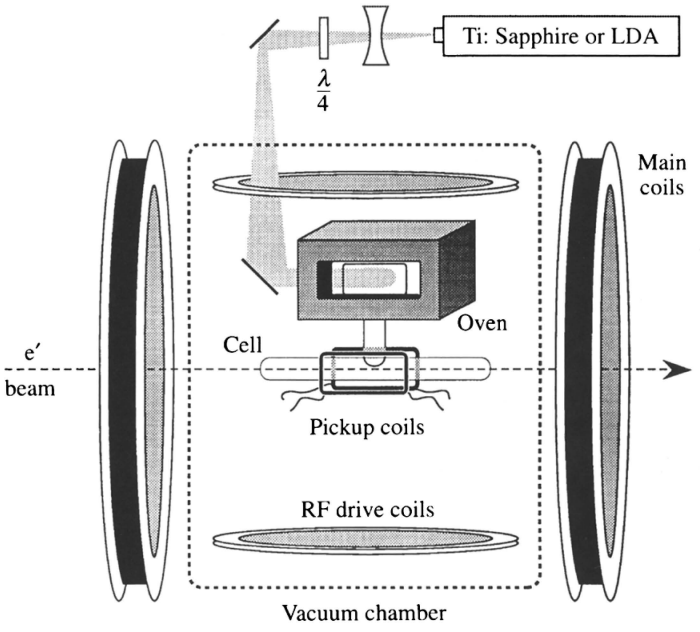

Fig. 6.9 The SLAC high-density gaseous polarized ^{3}He target (courtesy of J.R. Johnson).

$\mathscr{S}^\mu$, which was introduced in Section 3.4. Thus we begin with a study of the behaviour of $\mathscr{S}^\mu$ in the presence of macroscopic electric and magnetic fields.

6.3.1 Dynamics of the relativistic mean spin vector

Ehrenfest's theorem assures us that the motion of $\mathscr{S}^\mu$ is controlled in a classical fashion by the mean value of the interaction energy, which will involve the electric and magnetic fields.

Being macroscopic these fields do not vary on the scale of the particle's wave packet and so may be taken out of the mean value expressions. Thus the mean interaction energy may be constructed from the *given* classical field interacting with the *mean* spin vector $\mathscr{S}^\mu$.

In this section we shall deal exclusively with the *canonical* mean spin vector

$$\overset{\circ}{\mathscr{S}}{}^{\mu} = \frac{1}{s}(0, m\mathbf{s}) \tag{6.3.1}$$

where $\mathbf{s}$ is the mean spin vector in the canonical (comoving) rest frame reached from the frame where the particle of spin s has velocity $\mathbf{v}$ by the

https://doi.org/10.1017/9781009402040.006 Published online by Cambridge University Press

pure boost $l(\mathbf{v})$ (see Section 1.2). Then

$$\mathscr{S}^\mu = \Lambda^\mu{}_\nu[l(\mathbf{v})]\overset{\circ}{\mathscr{S}}{}^\nu = (\mathscr{S}^0, \boldsymbol{\mathcal{S}}) \tag{6.3.2}$$

so that $\mathscr{S}$ has the form

$$\begin{aligned} \boldsymbol{\mathcal{S}} &= \frac{1}{s}\left[\mathbf{s} + \frac{\gamma^2}{\gamma+1}(\boldsymbol{\beta}\cdot\mathbf{s})\boldsymbol{\beta}\right] \\ \mathscr{S}^0 &= \boldsymbol{\beta}\cdot\boldsymbol{\mathcal{S}} = \frac{\gamma}{s}(\boldsymbol{\beta}\cdot\mathbf{s}), \end{aligned} \tag{6.3.3}$$

the latter following from

$$p\cdot\mathscr{S} = 0. \tag{6.3.4}$$

We now seek a classical covariant equation for the rate of change of $\mathscr{S}^\mu$, with respect to the proper time τ, when it is acted upon by an arbitrary electromagnetic field specified by $F^{\mu\nu}$ in which the **E** and **B** fields are given by

$$\begin{aligned} E_j &= -F^{0j} \\ \epsilon^{ijk}B_k &= -F^{ij}. \end{aligned} \tag{6.3.5}$$

(In this subsection we use Gaussian units.)

Given that $\mathscr{S}^\mu$ is an axial vector, and assuming that $d\mathscr{S}^\mu/d\tau$ is linear in the fields and that it does not depend upon kinematic variables other than the 4-velocity

$$U^\mu = (\gamma c, \gamma\mathbf{v}) \tag{6.3.6}$$

and $\dot{U}^\mu \equiv dU^\mu/d\tau$, the most general form possible is

$$\frac{d\mathscr{S}^\mu}{d\tau} = aF^{\mu\nu}\mathscr{S}_\nu + b(\mathscr{S}_\alpha F^{\alpha\beta}U_\beta)U^\mu + d(\mathscr{S}_\alpha\dot{U}_\alpha)U^\mu \tag{6.3.7}$$

where a, b, d are constants.

The condition that $\mathscr{S}\cdot p = \mathscr{S}\cdot U = 0$ for all τ requires that

$$a = bc^2 \qquad d = -1/c^2 \tag{6.3.8}$$

if it is assumed that (6.3.7) holds no matter what sort of force causes the acceleration $\dot{U}^\mu$.

Finally we assume that for a particle at rest in a uniform magnetic field $\overset{\circ}{\mathbf{B}}$

$$\frac{d\mathbf{s}}{d\tau} = \text{ torque } = \boldsymbol{\mu}\times\overset{\circ}{\mathbf{B}}. \tag{6.3.9}$$

We write, for the magnetic moment,

$$\boldsymbol{\mu} = \frac{g\mu_0}{\hbar s}\mathbf{s} \tag{6.3.10}$$

https://doi.org/10.1017/9781009402040.006 Published online by Cambridge University Press

where for a particle of charge q

$$\mu_0 = \frac{q\hbar s}{2mc} \tag{6.3.11}$$

and where g is the gyromagnetic ratio.

Then

$$\frac{d\mathbf{s}}{d\tau} = \frac{g\mu_0}{\hbar s}\mathbf{s} \times \overset{\circ}{\mathbf{B}}. \tag{6.3.12}$$

Upon writing eqn (6.3.7) in the canonical rest frame, we recover (6.3.12) provided

$$a = g\mu_0. \tag{6.3.13}$$

Thus

$$\frac{d\mathscr{S}^\mu}{d\tau} = g\mu_0 \left[F^{\mu\nu}\mathscr{S}_\nu + \frac{1}{c^2}(\mathscr{S}_\alpha F^{\alpha\beta} U_\beta)U^\mu\right] - \frac{1}{c^2}(\mathscr{S}_\alpha \dot{\mathrm{U}}_\alpha)U^\mu. \tag{6.3.14}$$

If the particle is charged and if, in addition, its motion is largely controlled by the Lorentz-force interaction with the electromagnetic fields then

$$\frac{d\mathbf{p}}{dt} = q[\mathbf{E} + (\boldsymbol{\beta} \times \mathbf{B})] \tag{6.3.15}$$

and

$$\frac{dp_0}{dt} = q\boldsymbol{\beta} \cdot \mathbf{E}, \tag{6.3.16}$$

which, since $p^\mu = mU^\mu$ (p^μ is the kinetic, not the canonical, 4-momentum), can be written as

$$\dot{U}^\mu \equiv \frac{dU^\mu}{d\tau} = \frac{q}{mc}F^{\mu\nu}U_\nu. \tag{6.3.17}$$

In this case (6.3.14) becomes the celebrated Thomas–BMT equation:

$$\frac{d\mathscr{S}^\mu}{d\tau} = \frac{q}{mc}\left[\frac{g}{2}F^{\mu\nu}\mathscr{S}_\nu + \frac{1}{c^2}\left(\frac{g}{2} - 1\right)(\mathscr{S}_\alpha F^{\alpha\beta}U_\beta)U^\mu\right] \tag{6.3.18}$$

(Thomas, 1927; Bargmann, Michel and Telegdi, 1959). In (6.3.18) it is clear that $g = 2$ is a very special value.

Before turning to the question of the spin motion in an accelerator it is instructive to use (6.3.14) to rederive the Thomas precession dealt with in subsection 2.2.8.

We are interested in the rate of change of the canonical rest system $\mathbf{s}$ with laboratory time t. Substitution of (6.3.3) into (6.3.14) followed by a

https://doi.org/10.1017/9781009402040.006 Published online by Cambridge University Press

daunting piece of algebra leads to

$$\frac{d\mathbf{s}}{dt} = \mathbf{s} \times \left\{ \frac{g\mu_0}{\hbar s} \left[\mathbf{B} - \frac{\gamma}{\gamma + 1} (\boldsymbol{\beta} \cdot \mathbf{B}) \boldsymbol{\beta} - \boldsymbol{\beta} \times \mathbf{E} \right] + \frac{\gamma^2}{\gamma + 1} \boldsymbol{\beta} \times \frac{d\boldsymbol{\beta}}{dt} \right\}. \tag{6.3.19}$$

For the case of a pure electric field (the Coulomb field of the nucleus) and with $\mu_0 = -e\hbar s/(2mc)$ for an electron, (6.3.19) becomes

$$\frac{d\mathbf{s}}{dt} = \frac{ge}{2mc^2} \mathbf{s} \times (\mathbf{v} \times \mathbf{E}) + \boldsymbol{\omega}_{\mathrm{T}} \times \mathbf{s} \tag{6.3.20}$$

where, in terms of the acceleration $\mathbf{a}$,

$$\boldsymbol{\omega}_{\mathrm{T}} = \frac{1}{c^2} \left(\frac{\gamma^2}{\gamma + 1} \right) (\mathbf{a} \times \mathbf{v})$$

in agreement with eqns (2.2.34), (2.2.35).

When the motion of a charged particle is controlled by the Lorentz force, (6.3.15) and (6.3.16) yield for the acceleration

$$\frac{d\boldsymbol{\beta}}{dt} = \frac{q}{\gamma mc} [\mathbf{E} + \boldsymbol{\beta} \times \mathbf{B} - (\boldsymbol{\beta} \cdot \mathbf{E}) \boldsymbol{\beta}], \tag{6.3.21}$$

which, substituted into (6.3.19), gives

$$\frac{d\mathbf{s}}{dt} = \frac{q}{mc} \mathbf{s} \times \left[\left(\frac{g}{2} - 1 + \frac{1}{\gamma} \right) \mathbf{B} - \left(\frac{g}{2} - 1 \right) \frac{\gamma}{\gamma + 1} (\boldsymbol{\beta} \cdot \mathbf{B}) \boldsymbol{\beta} - \left(\frac{g}{2} - 1 + \frac{1}{\gamma + 1} \right) \boldsymbol{\beta} \times \mathbf{E} \right]. \tag{6.3.22}$$

6.3.2 *Difficulties in the acceleration of polarized particles*

We shall utilize eqn (6.3.22) to give a brief explanation of the problems that occur when one attempts to accelerate polarized particles. We consider protons being accelerated in a planar circular accelerator whose guide field $\mathbf{B}_0$ is in the OZ direction, so that the equilibrium orbit lies in the XY-plane. In this case, in (6.3.22) $\mathbf{E} = 0$ and $\boldsymbol{\beta} \perp \mathbf{B}_0$, so that

$$\frac{d\mathbf{s}}{dt} = -\frac{q}{mc} \left(\frac{g}{2} - 1 + \frac{1}{\gamma} \right) \mathbf{B}_0 \times \mathbf{s} \tag{6.3.23}$$

and (6.3.21) becomes

$$\frac{d\boldsymbol{\beta}}{dt} = -\frac{q}{\gamma mc} \mathbf{B}_0 \times \boldsymbol{\beta}. \tag{6.3.24}$$

https://doi.org/10.1017/9781009402040.006 Published online by Cambridge University Press

Since $g/2 > 1$ both $\mathbf{s}$ and $\boldsymbol{\beta}$ rotate about $\mathbf{B}_0$ in the same sense, with angular frequences as follows.

$$\begin{aligned} &\text{For } \boldsymbol{\beta}: \quad \Omega_c = \text{ relativistic cyclotron frequency } = -\frac{q}{\gamma mc} B_0. \\ &\text{For } \mathbf{s}: \quad \Omega_s = -\frac{q}{mc}\left(G + \frac{1}{\gamma}\right) B_0 = (\gamma G + 1)\Omega_c, \end{aligned} \tag{6.3.25}$$

where

$$G = g/2 - 1 \tag{6.3.26}$$

is called the *gyromagnetic anomaly*.

The difference in angular frequencies is then

$$\Omega \equiv \Omega_s - \Omega_c = -\frac{qG}{mc} B_0 = \Omega_c G\gamma. \tag{6.3.27}$$

Thus the quantity $G\gamma$ measures how much bigger Ω is than Ω_c in a frame that rotates with the velocity vector. It thus measures the number of complete spin precessions in this frame per revolution of the particle in its orbit. It is known as the *spin tune* and is often written ν_s.

Note that for protons $G = 1.79$, so that in a high energy accelerator $G\gamma$ is a large number. For electrons G is exceedingly small, $G \approx 1.16 \times 10^{-3}$, but at LEP or HERA γ is very large, so that again $G\gamma$ is large (≈ 103 at the Z^0 mass at LEP, ≈ 63 at HERA). This means, via (6.3.27), that if the beam direction is altered by a small angle as a consequence of passing through some field $\mathbf{B}$, then the component of the mean spin vector perpendicular to $\mathbf{B}$ will rotate through a much larger angle, namely $1 + G\gamma$ times larger.

In a perfect machine, with all particles moving along the equilibrium orbit of radius R and with uniform $\mathbf{B} = B_0\mathbf{e}_z$ the mean spin $\mathbf{s}$ would simply precess about the Z-axis.

It should be remembered that the Ωs are not constant but are functions of time. For example, the equilibrium orbit is given by

$$r = R = \frac{v\gamma mc}{qB_0} \tag{6.3.28}$$

and is constant in a synchrotron, so that

$$|\Omega_c| = v/R \tag{6.3.29}$$

increases as the particle accelerates.

There are three main effects that disturb the ideal situation in a synchrotron:

https://doi.org/10.1017/9781009402040.006 Published online by Cambridge University Press

(i) the quadrupole fields that focus the beam have a component of **B** in the horizontal plane and the component B_z varies in the radial direction;
(ii) there are imperfections in the fields due to misaligment of magnets, field errors etc.;
(iii) spin-flip occurs as a result of synchrotron radiation.

The latter is very important for electron machines and will be dealt with in Section 7.1. We shall ignore it in discussing proton accelerators.

(i) Consider protons injected into an accelerator with all spins parallel to OZ, so that initially the beam is 100% polarized. A particle that is not moving along the equilibrium orbit $r = R$, $z = 0$ experiences vertical and horizontal focussing forces that cause it to oscillate about the equilibrium orbit. These vertical and horizontal *betatron oscillations* have frequencies that depend upon the *field index n*, which, to first order, describes how $B_z(r)$ varies near $r = R$. That is, n is defined by writing

$$B_z(R + \delta r) = B_0 \left(1 - \frac{n\delta r}{R}\right) \tag{6.3.30}$$

where $B_0 \equiv B_z(R)$.

Because of these perturbations, after each revolution **s** will differ slightly from the value given by eqn (6.3.23). Since **s** is initially along OZ it is not affected by the fact that B_z varies with r. However, it will precess around the horizontal components of **B** during its vertical betatron oscillations.

In a system of perfect magnets these precessions would average to zero. But in reality there are always stray horizontal fields at the end of any magnet or group of magnets and the strength of these fields will vary with z. Thus when a particle traverses the gap between such magnets while undergoing vertical betatron oscillations, **s** will pick up a net non-zero precession about the horizontal axes along and perpendicular to the beam.

Because of the weakness of the horizontal fields, the effect, per revolution, is very small. But large resonant results can build up if the small perturbations are in phase.

Let Q_z be the *vertical tune*, i.e. the number of vertical betatron oscillations per revolution, and let the accelerator have a K-fold symmetry. Then, using eqn (6.3.22) with the horizontal fields included, putting $\mathbf{s} = \mathbf{s}_0 + \Delta\mathbf{s}$, where $\mathbf{s}_0(t)$ is the mean spin vector in the presence of the uniform field $\mathbf{B}_0$, and keeping only terms linear in $\Delta\mathbf{s}$ in the resulting equation one finds (Froissart and Stora, 1959) that the condition for resonance is

$$\nu_s \equiv \gamma G = mK \pm Q_z \qquad m = \text{ integer.} \tag{6.3.31}$$

https://doi.org/10.1017/9781009402040.006 Published online by Cambridge University Press

Equation (6.3.31) can be understood intuitively as follows. The horizontal components of **s** involve the oscillatory functions $\cos\Omega t$, $\sin\Omega t$. These are subject to a perturbation that depends upon the vertical betatron oscillations and thus involves $\cos(Q_z\Omega_c t)$, $\sin(Q_z\Omega_c t)$. The angular frequencies involved in the product of such terms are then $\Omega \pm Q_z\Omega_c$, and the times at which the perturbation acts are $t_N = N\tau/K$, where τ, the period of revolution, is given by $2\pi/\Omega_c$. For a resonant build-up we require that the phases of the resultant angular functions change by $2m\pi$ when $N \to N+1$. Thus we require

$$(\Omega \pm Q_z\Omega_c)\frac{2\pi}{K\Omega_c} = 2m\pi,$$

which yields (6.3.31) immediately.

The above resonances are known as *intrinsic resonances.*

(ii) Because of imperfections in the magnetic field even the equilibrium orbit will not be the idealized circle we have been assuming. However, since the real orbit is closed, the path must retrace itself each revolution. The imperfection causes a small change in the expected **s** and once again this will build up resonantly if the spin precession is in phase with the time of encountering the imperfection. This will occur whenever $G\gamma$ is an integer. These resonances are the *imperfection resonances.* They occur at energies given by

$$E = m\gamma c^2 = \left(\frac{mc^2}{G}\right)G\gamma = \left(\frac{mc^2}{G}\right) \times \text{ integer} \qquad (6.3.32)$$

so that the spacing is

$$\Delta E = \left(\frac{mc^2}{G}\right), \qquad (6.3.33)$$

which for protons ($G = 1.79$) is ≈ 523 MeV.

In both the above mechanisms, the resonance conditions depend upon the energy of the particle. Of course the actual consequence of a given resonance will depend upon the details of the particular accelerator. But what appears inevitable in the above is that in the process of accelerating to higher and higher energies the particle will encounter an ever growing number of depolarizing resonances of varying strength. The challenge is to find a way to 'jump' or 'cross' these resonances with as little loss of polarization as possible.

A traditional method, pioneered at the Argonne ZGS, is to use pulsed quadrupole magnets to induce a rapid change in Q_z while the beam energy is in the vicinity of a resonance value. The choice of pulse duration, timing and strength seems to be an art. Figure 6.10 shows the degree

of polarization as the beam momentum increases in the ZGS with and without the pulsed quadrupoles. The results are dramatic!

However, each resonance has to be studied separately so that, as the accelerator output energy goes up and the number of resonances encountered increases more or less proportionately to the energy, this becomes an extremely difficult task, with thousands of resonances to be manipulated.

A wonderful solution to the above was suggested many years ago (in 1976!) but only now appears to have become a practical tool: the Siberian snake, which we now discuss.

6.3.3 The Siberian snake

A radical solution to the above problem is provided by the Siberian snake (Derbenev and Kondratenko, 1976), in which **s** is rotated through 180° around a horizontal axis each revolution, with a consequent cancelling-out of the depolarizing effects.

Moreover the arrangement can be made independent of energy so that the spin tune ν_s is a fixed number, a half-integer, and all integer spin resonances have disappeared!

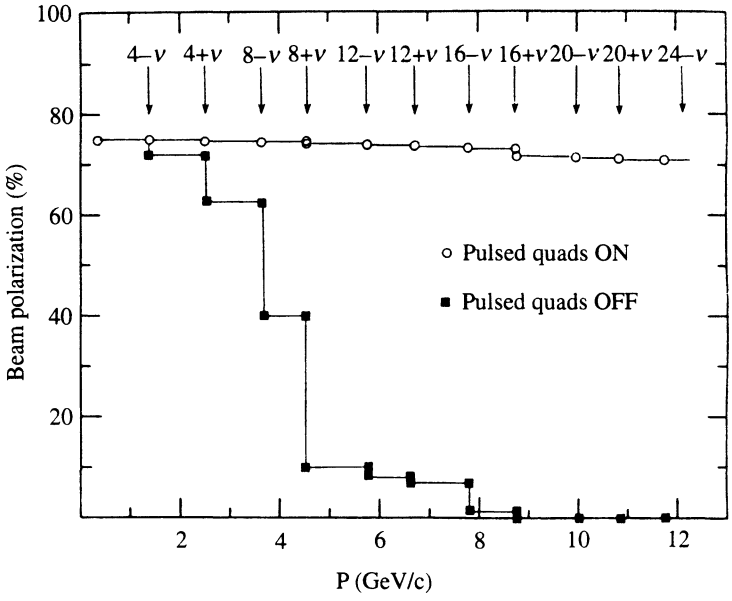

Fig. 6.10 Beam polarization as a function of momentum, as various resonances are crossed at the ZGS (from Fernow and Krisch, 1981).

https://doi.org/10.1017/9781009402040.006 Published online by Cambridge University Press

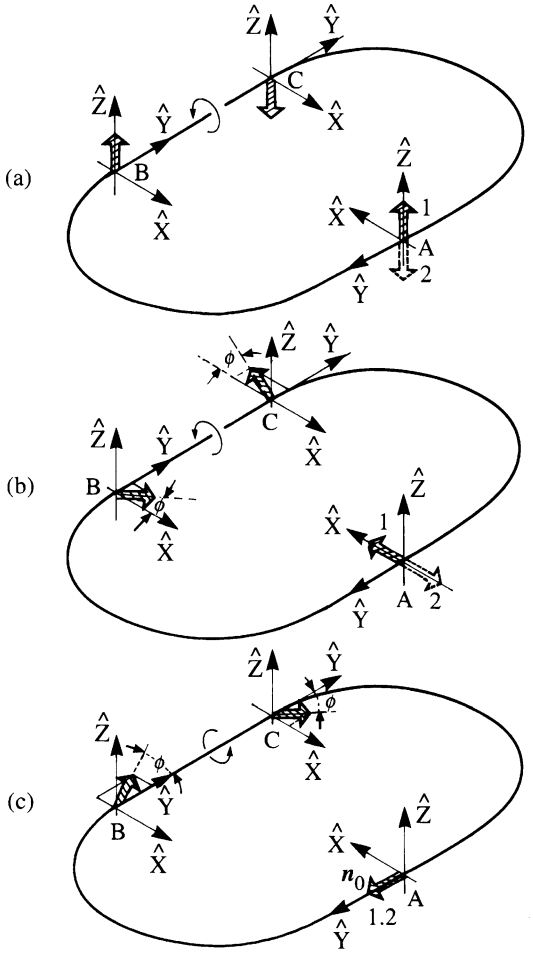

Fig. 6.11 Precession of various spin vectors through a Siberian snake on a particle's path $A \to B \to C \to A$: (a) $\mathbf{s}_A^z$; (b) $\mathbf{s}_A^x$; (c) $\mathbf{s}_A^y$.

The functioning of a Siberian snake can be understood pictorially in Fig. 6.11, which has been adapted from the review article of Montague (1984). We refer everything to the frame $\hat{X}\hat{Y}\hat{Z}$ attached to the particle, with $O\hat{Y}$ along the velocity and $O\hat{Z}$ perpendicular to the plane of the accelerator, and we consider what happens to the mean spin vector $\mathbf{s}_A$ at A as the particle makes one revolution on its orbit. The Siberian snake 'mechanism' is installed in the section BC and, in this version, consists of a longitudinal magnetic field, i.e. a field along the particle's motion. We assume a vertical guide field $B_0\mathbf{e}_z$ along the semicircular sections of the orbit.

https://doi.org/10.1017/9781009402040.006 Published online by Cambridge University Press

At A we resolve $\mathbf{s}_A$ into orthogonal vectors $\mathbf{s}_A^j$, lying along the axes at A, and follow the precession of each component vector (shown hatched) separately. These precessions along the path $A \to B \to C \to A$ are shown in Fig. 6.11(a), (b), (c) respectively. To understand what happens between B and C let us return to eqn (6.3.22) for the case where $\mathbf{B} = \mathbf{b}_\parallel$ is along the motion. Then

$$\frac{d\mathbf{s}}{dt} = \left(\frac{q}{mc\gamma}\right)\frac{g}{2}\mathbf{s} \times \mathbf{b}_\parallel \tag{6.3.34}$$

and $\mathbf{s}$ precesses about its velocity vector $\boldsymbol{\beta}$ with angular frequency

$$\Omega_\parallel = -\frac{qgb_\parallel}{2mc\gamma}. \tag{6.3.35}$$

We suppose that $b_\parallel$ is adjusted so that the rotation angle about $\boldsymbol{\beta}$ between B and C is 180°.

Consider, in Fig. 6.11(a), the precession of $\mathbf{s}_A^z$. Along $A \to B$ it is parallel to the guide field, so reaches B unaltered. Along $B \to C$ it rotates about $O\hat{Y}$ by 180° then returns to A antiparallel to $O\hat{Z}$. In (b) we follow $\mathbf{s}_A^x$. Along $A \to B$ it rotates about $O\hat{Z}$ at angular frequency $\Omega = \Omega_c G\gamma$; see (6.3.27). The $O\hat{X}$ axis has turned through angle $\Omega_c t = \pi$, so the precession angle is $G\gamma\pi$ which we write as $2N\pi - \phi$, so that at B $\mathbf{s}_A^x$ makes an angle ϕ with $O\hat{X}$ as shown. On $B \to C$ it rotates about $\boldsymbol{\beta}$ by 180°, ending up at C with the orientation shown. From $C \to A$ it precesses through $2N\pi - \phi$ degrees so that at A it is antiparallel to $O\hat{X}$. Finally in (c) we follow $\mathbf{s}_A^y$ and find that it ends up parallel to $O\hat{Y}$ at A. Thus $\mathbf{s}_A$ rotates about its velocity by 180° per revolution.

Although suggested in 1976, the practical construction of a Siberian snake is a non-trivial matter and the first ever was tested at Indiana only a few years ago (Krisch *et al.*, 1989). The results shown in Fig. 6.12 plot the beam degree of polarization against a quantity that controls the strength of an imperfection resonance. Without the snake the degree of polarization drops rapidly as a function of the strength of the imperfection. With the snake on, the polarization remains essentially unchanged. The above experiment was carried out at fixed beam momentum.

It seems that to overcome imperfection resonances a 'partial' snake, which does not rotate the spin through a full 180°, is adequate, but the full snake is required for intrinsic resonances. Experiments at Indiana have continued with great success, including the overcoming of the depolarization from overlapping depolarizing resonances. A Siberian snake has also been built at the Brookhaven AGS with very encouraging results (Huang and Roser, 1994) and is being incorporated in the chain that produces polarized protons in RHIC. A partial snake will overcome all

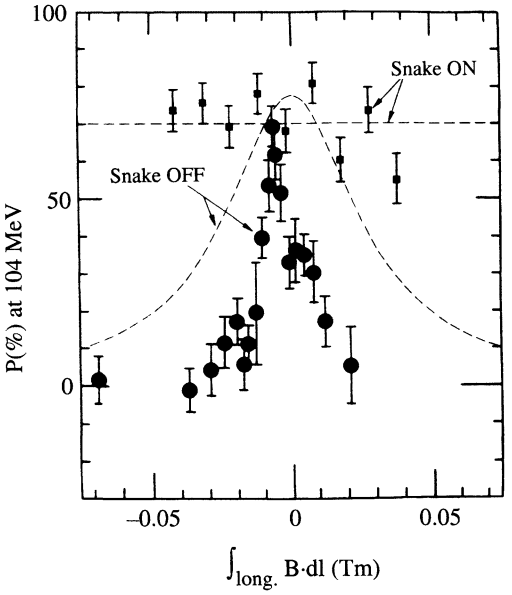

Fig. 6.12 First test of the Siberian snake. See text; the curve gives the theoretical resonance shape (from Krisch *et al.*, 1989).

imperfection resonances during acceleration up to 24 GeV in the AGS, while the six main intrinsic resonances encountered will be corrected by the pulsed quadrupole method. After transfer to the RHIC accelerator the beam will pass through four split Siberian snakes, as shown in Fig. 6.13. This configuration should preserve the polarization up to an energy per beam of 250 GeV. The expected beam polarization is 70%.

6.3.4 Stern–Gerlach polarization of protons and antiprotons

Finally we give a brief outline of a totally new approach to the production of polarized protons and antiprotons, which, however, has not yet been shown to be a practical tool but which seems promising.

The idea is to avoid all the problems encountered when accelerating polarized particles in a circular accelerator, by first accelerating unpolarized particles and then polarizing them while they circulate at fixed energy in a storage ring. It would permit the fantastic possibility of a high energy polarized antiproton beam.

The basic idea is the following (Niinikoski and Rossmanith, 1985). The beam in a storage ring is focussed by alternate quadrupoles of opposite polarity. Normally one considers only the effect on the motion due to the charge, but each quadrupole will, in addition, give rise to a tiny Stern–

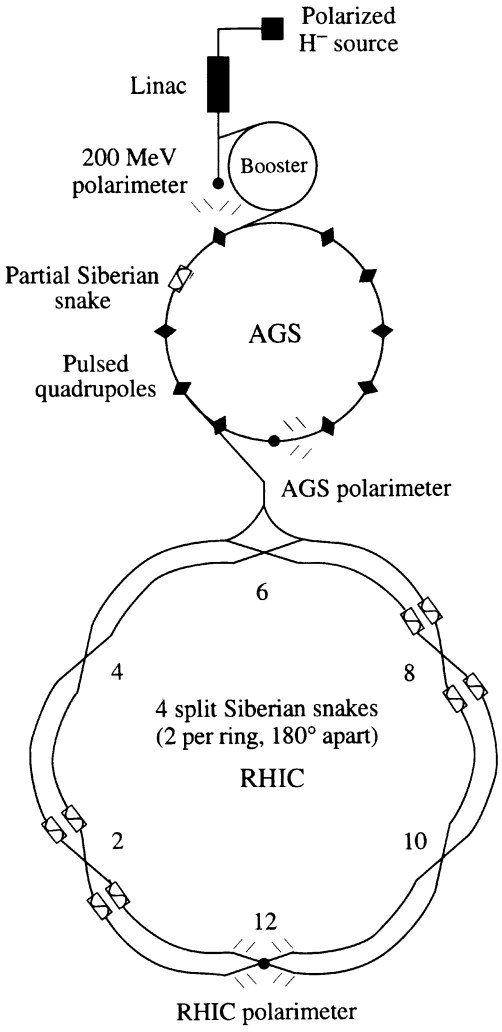

Fig. 6.13 Lay-out of the RHIC accelerator showing the Siberian snakes (from Bunce *et al.*, 1992).

Gerlach splitting of the beam. (For this reason the phenomenon has been christened the *spin-splitter* effect.)

With the system of axes indicated, the field of the quadrupole shown in Fig. 6.14 near its central axis is given approximately by

$$B_x = by \qquad B_y = bx \tag{6.3.36}$$

where b is called the radial field gradient. The beam is travelling in the OZ direction and the force on an arbitrary magnetic moment $\boldsymbol{\mu}$ has

https://doi.org/10.1017/9781009402040.006 Published online by Cambridge University Press

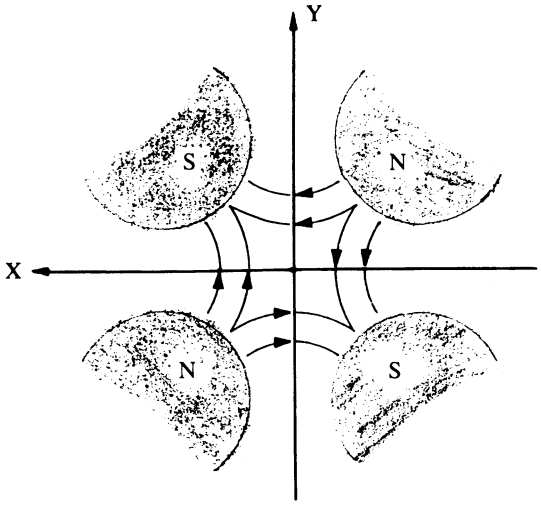

Fig. 6.14. Schematic picture of the field of a magnetic quadrupole.

components

$$F_x = b\mu_y \qquad F_y = b\mu_x. \tag{6.3.37}$$

For alternate quadrupoles b changes sign, so that the direction of the force on $\boldsymbol{\mu}$ alternates from one quadrupole to the next.

Each quadrupole of length L will generate an additional angular deflection δ of order

$$\delta \approx \frac{b\mu L}{E}. \tag{6.3.38}$$

For typical gradients ≈ 10 T/m and $L \approx 1$ m one has

$$\delta \approx \frac{10^{-13}}{E(\text{GeV}) \text{ radians}}. \tag{6.3.39}$$

This seems a hopelessly small angle. However, if the sequence of deflections can be phased to add up coherently then it has been suggested that it might be possible to build up a spatial separation in the beam, between particles of opposite spin direction, of the order of a few millimetres in a period of about 1 hour.

If the spin did not precess between the quadrupoles of opposite polarity then there would be an effective cancelling-out of deflections. Thus we require that $\boldsymbol{\mu}$ precesses by a rotation angle that is an odd number of π radians during the passage from one quadrupole to the next. This could be the normal precession around the guide field between quadrupoles, which would give rise to a reversal of μ_x and hence, by (6.3.37), to a coherent

https://doi.org/10.1017/9781009402040.006 Published online by Cambridge University Press

build-up of a vertical separation between particles of opposite μ_x, i.e. of opposite transverse, *horizontal*, components of spin.

We are trying to build up a displacement vertically by means of periodic impulse from the quadrupoles. At the same time the particle is undergoing vertical betatron oscillations. Clearly to ensure a resonant build-up, revolution by revolution, we require the spin precession to be in phase with the vertical betatron oscillations. This is just the condition (6.3.31), which, ironically, as discussed in subsection 6.3.2 is the condition for an intrinsic resonance causing depolarization of the *vertical* component of the spin.

A slightly modified scheme to polarize antiprotons at the low energy CERN LEAR collider was proposed by Onel, Penzo and Rossmanith (1986) in which the spin precession between quadrupoles was to be caused by a Siberian snake in which $\boldsymbol{\mu}$ rotates about a longitudinal **B**-field. For a momentum of 200 MeV/c and $b = 20$ T/m it was estimated that a separation of 2.5 mm per hour could be built up. Unfortunately this scheme was never brought to fruition. It seems unrealistic in practice to try to have complete separation of the beams, especially given that the effect decreases with energy; see (6.3.39). In the time involved (hours) several other effects could destroy the build-up of polarization, e.g. depolarization due to imperfections, intrabeam scattering, fluctuations in power supplies etc. Thus the original idea does not seem practicable.

However, there are two new developments that suggest that a practicable scheme may be possible. The first idea does not directly resolve the difficulties but it does allow for a more flexible approach to the type of spin-based separation created.

Conte, Penzo and Pusterla (Conte *et al.*, 1995) argued that the use of longitudinal magnetic fields, with a field gradient along the particle's trajectory, induces tiny longitudinal forces that will result in minute changes ΔE of the kinetic energy of the particle. These changes will be negative or positive, depending on the sign of the longitudinal component of $\boldsymbol{\mu}$, and could be used to create a longitudinal separation in the beam that is correlated to the spin direction. In this case the effect does not decrease with energy, but, like the vertical or horizontal separation discussed earlier, it may be impractical to generate a utilizable separation in a reasonable time span.

The second idea is due to Derbenev (1990) and relies on a concept of resonant enhancement of the small splitting effects. For the vertical or horizontal splitting the particle is undergoing betatron oscillations whose phase is related to the spin direction. For the case of longitudinal separation the magnetic gradient could be provided by passing the beam through a transverse electric (TE) cavity, thus generating an oscillatory energy change ΔE whose phase is again linked to the spin direction. This would give rise to small induced coherent synchrotron oscillations in

addition to the usual incoherent ones. If now a detector is constructed to measure either kind of oscillation it can be used to drive a feedback system that will apply a suitable rf field, leading to a resonant enhancement of the effect. Estimates suggest that significant polarization could be achieved in a few minutes. A practical scheme is discussed in Akchurin *et al.* (1996).

6.4 Polarized secondary and tertiary beams

It is a mysterious empirical fact that hyperons produced with medium momentum transfer in the collision of an unpolarized proton beam with an unpolarized hydrogen or nuclear target emerge with a significant degree of polarization. Moreover, the polarization is largely independent of the

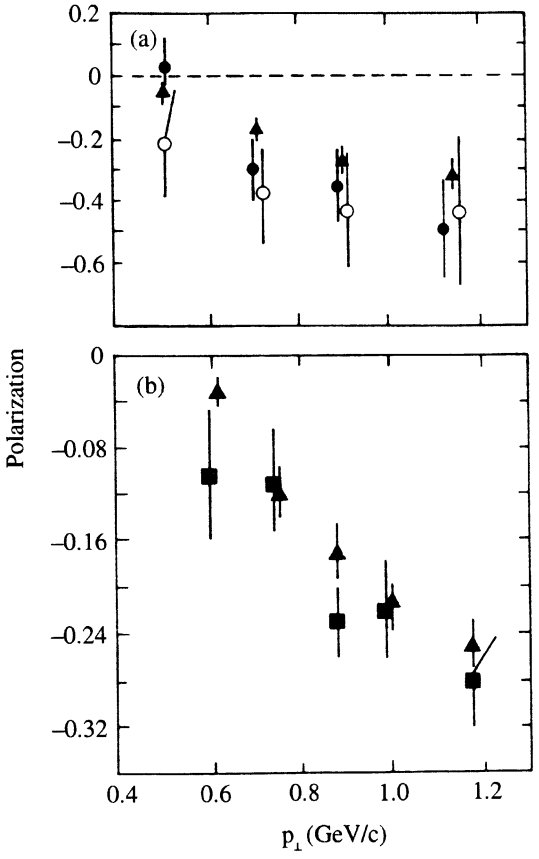

Fig. 6.15. Polarization of inclusive Λ production at several energies vs. $p_\perp$. (a) $p+N \rightarrow \Lambda^0+X$: ▲, 400 GeV; •, 1500 GeV; ○, 2000 GeV. (b) ▲, 400 GeV H_2; ■, 28 GeV H_2 or D_2. The five sets of points in (b) correspond to x_F-values, from left to right, of 0.36, 0.45, 0.52, 0.59 and 0.69.

https://doi.org/10.1017/9781009402040.006 Published online by Cambridge University Press

collision energy over a wide range, as shown for Λ particles in Fig. 6.15. The dependence of the polarization upon the type of hyperon produced, for the $p - Be$ reaction at $P_{\text{Lab}} = 400$ GeV/c and at a fixed Lab angle of 5 mrad, is shown in Fig. 6.16 plotted against the Lab momentum of the produced hyperon. It is seen that there is a significant polarization for Λ, Σ^+, Ξ^-. There is no convincing theoretical explanation for this polarization, as will be discussed in Chapter 13.

It has proved possible at Fermilab to utilize these secondary polarized hyperons in further interactions in which tertiary hyperons are produced. By analysing the decay distribution of the latter, one can measure the depolarization or polarization transfer parameters for reaction of the type

$$\text{hyperon} + \text{nucleus} \rightarrow \text{hyperon} + X.$$

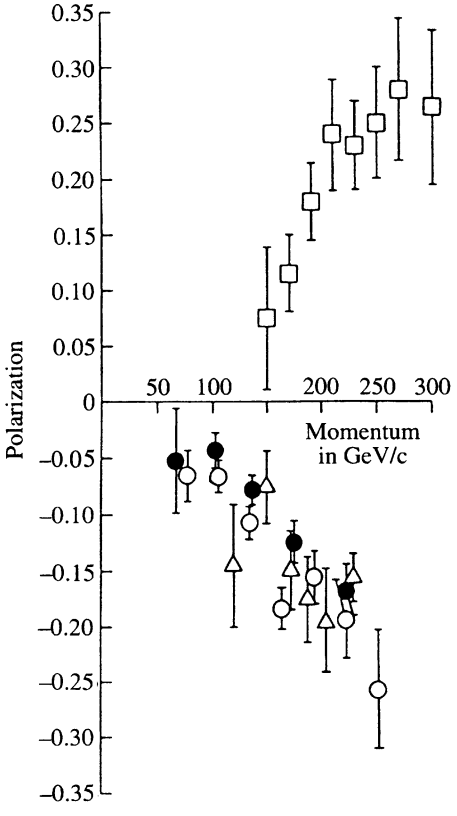

Fig. 6.16 Polarization in inclusive hyperon production at 400 GeV/c at a fixed Lab angle of 5 mrad: ○, $p + \text{Be} \rightarrow \Lambda^0 + X$; ●, $p + p \rightarrow \Lambda^0 + X$; △, $p + \text{Be} \rightarrow \Xi^- + X$; □, $p + \text{Be} \rightarrow \Sigma^+ + X$.

https://doi.org/10.1017/9781009402040.006 Published online by Cambridge University Press

Almost at the boundary of science fiction are experiments at Fermilab on the production of Ω^- (Longo *et al.*, 1989). Using 800 GeV/c unpolarized protons on a beryllium target, a sample of about 100 000 Ωs was obtained and was found to have essentially zero polarization; see Fig. 6.17.

When instead a secondary beam consisting of a mixture of polarized Λs and Ξ^0s strikes a copper target the produced Ωs are found to be significantly polarized! (See Fig. 6.18.) At the time of the Minneapolis Conference (1988) some 20 000 polarized Ωs had been produced in this way and had been allowed to precess in a magnetic field so as to allow the first ever measurement of their magnetic moment. By now (the year 2001) the magnetic moment is known with some precision,

$$\mu(\Omega) = (-2.02 \pm 0.05)\mu_N,$$

in nuclear magnetons; this is a result of importance in testing the constituent quark model of the hadrons.

One of the most beautiful developments in recent years has been the construction of very energetic, highly polarized, *tertiary* proton and an-

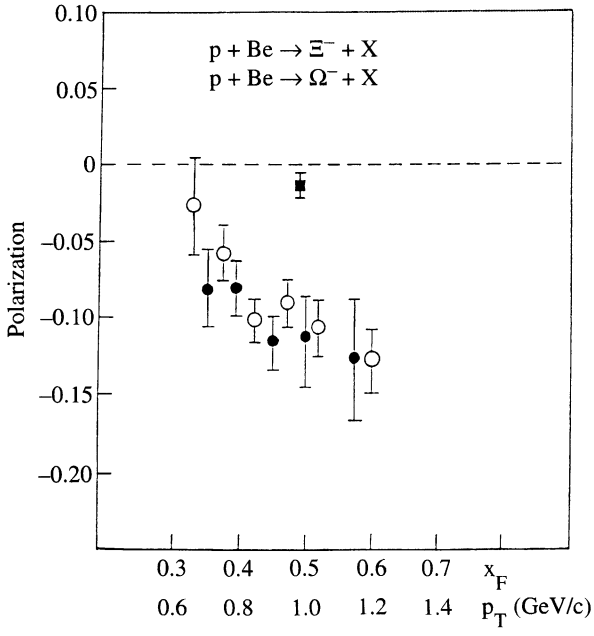

Fig. 6.17 Comparison of Ξ and Ω polarization in inclusive hyperon production on beryllium (from Longo *et al.*, 1989): ○, Ξ_- at 400 GeV, 5 mrad; ●, Ξ^- at 800 GeV, 2.5 mrad; , Ω^- at 800 GeV, 2.5 mrad.

https://doi.org/10.1017/9781009402040.006 Published online by Cambridge University Press

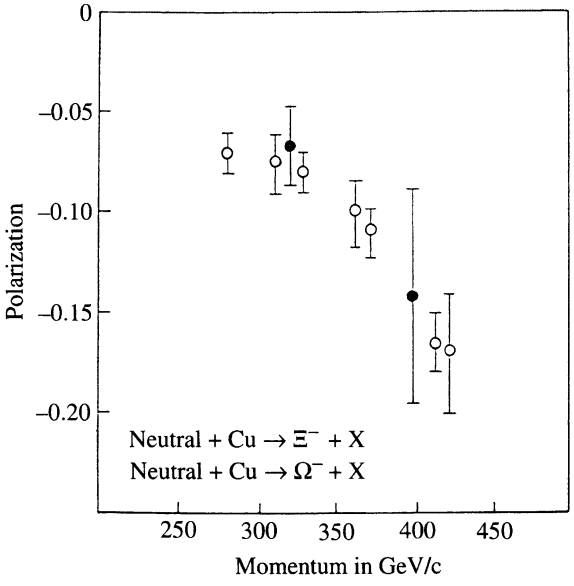

Fig. 6.18 Polarization of Ωs produced when a polarized hyperon beam strikes a copper target (from Longo *et al.*, 1989): ○, Ξ^-; ●, Ω^-.

tiproton beams at Fermilab (Grosnick *et al.*, 1990). To be specific, we shall discuss the proton beam; the antiproton case is analogous.

Protons of momentum 800 GeV/c from the Fermilab Tevatron strike a beryllium target and produce copious numbers of approximately forward-going Λs. The forward-going Λs must be unpolarized on account of eqns (3.1.35), (5.4.2) and (5.3.18b). However, their decay in flight into $p\pi^-$ is parity violating and the protons are produced with a longitudinal polarization $\mathscr{P} \approx 64\%$ (see subsection 8.2.1).

The spin-polarization vector $\mathcal{P}$ is shown in Fig. 6.19 in the helicity rest frame S_p of the proton as reached from the helicity rest frame S_Λ of the Λ particle. The proton is produced at an angle θ in S_Λ, as shown, and with energy

$$E = \frac{m_\Lambda^2 + m^2 - \mu^2}{2m_\Lambda} \approx 943 \text{ MeV}$$

and magnitude of momentum

$$p = \frac{\left\{\left[(m_\Lambda + m)^2 - \mu^2\right]\left[(m_\Lambda - m)^2 - \mu^2\right]\right\}^{1/2}}{2m_\Lambda} \approx 101 \text{ MeV}/c.$$

https://doi.org/10.1017/9781009402040.006 Published online by Cambridge University Press

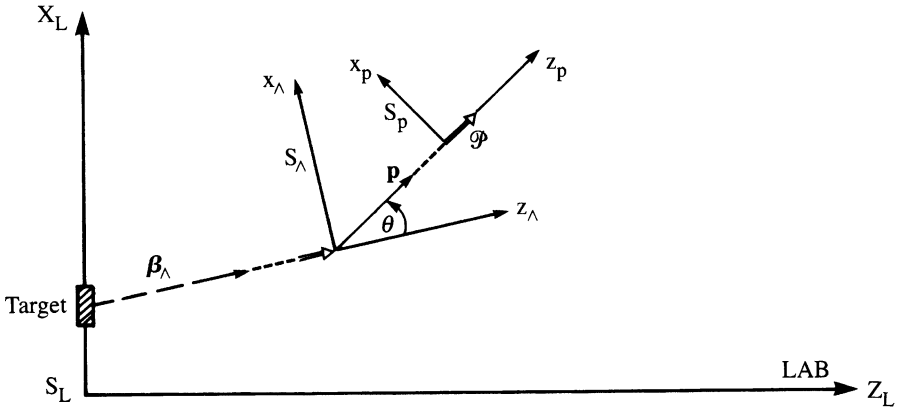

Fig. 6.19 The decay $\Lambda \to p\pi^-$ showing the Λ helicity rest frame S_Λ and the proton helicity rest frame S_p as reached from S_Λ. The proton has momentum $\mathbf{p}$ in S_Λ. $\mathscr{P}$ is the spin-polarization vector.

The spin-polarization vector $\mathcal{P}$ lies along OZ_p in the proton's helicity rest frame. Note that the proton is almost completely non-relativistic in the rest frame S_Λ.

Viewed in the Lab we have then the picture shown in Fig. 6.20, in which S'_p is the proton's helicity rest frame as reached from the laboratory frame. One has

$$p_L \sin\theta' = p \sin\theta \tag{6.4.1}$$

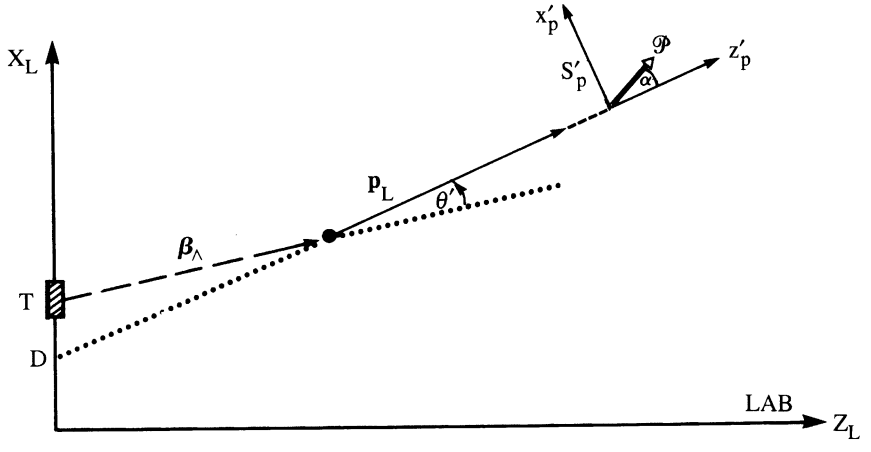

Fig. 6.20 The decay $\Lambda \to p\pi^-$ in the Lab. S'_p is the proton helicity rest frame reached from the Lab, where the proton has momentum $\mathbf{p}_L$. $\mathscr{P}$ makes an angle α with OZ'_p.

https://doi.org/10.1017/9781009402040.006 Published online by Cambridge University Press

where p_L is the magnitude of the proton's Lab momentum and is ≈ 185 GeV/c.

The boost of axes $l(\boldsymbol{\beta})$ with $\boldsymbol{\beta} = -\boldsymbol{\beta}_\Lambda$ that takes us to the Lab induces a Wick helicity rotation on the spin-polarization vector so that $\mathcal{P}$, which was along OZ_p in S_p is now at an angle α to OZ'_p of S'_p; from (2.2.9), (2.2.6) and (3.2.10) $\alpha = -\theta_{\text{Wick}}$ is given by

$$\begin{aligned}\sin\alpha &= \frac{m}{p_L}\gamma_\Lambda\beta_\Lambda \sin\theta \\ &= \frac{m}{m_\Lambda}\frac{p_\Lambda}{p_L}\sin\theta\end{aligned}$$

and using (6.4.1)

$$\sin\alpha = \frac{m}{m_\Lambda}\frac{p_\Lambda}{p}\sin\theta'. \tag{6.4.2}$$

The component of the spin-polarization vector *transverse* to the proton's motion is

$$\begin{aligned}\mathcal{P}_T &= \mathcal{P}\sin\alpha \\ &= \mathcal{P}\frac{m}{m_\Lambda}\frac{p_\Lambda}{p}\sin\theta'.\end{aligned} \tag{6.4.3}$$

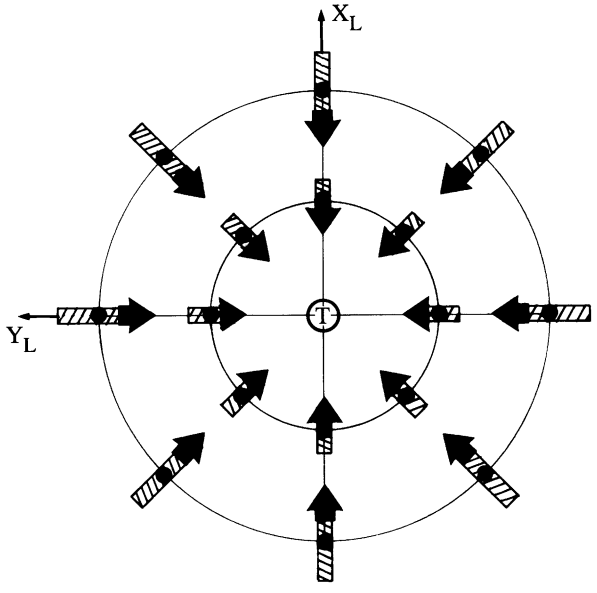

Fig. 6.21 Correlation between the magnitude and direction of the transverse component of the proton's spin-polarization vector and the position of the virtual source in the $X_L Y_L$-plane. The solid circles give the positions to which the spin-polarization vectors refer.

https://doi.org/10.1017/9781009402040.006 Published online by Cambridge University Press

Moreover the geometry is such that θ' is an extremely small angle, so that if the line of motion of the proton is projected backwards until it reaches the plane of the target at D, as shown in Fig. 6.20, then

$$DT = L\theta' \tag{6.4.4}$$

where L is the distance covered by the Λs before decaying.

Thus we see that $\mathcal{P}_T$ is proportional to the distance from the target to the 'virtual source' D of the protons in the Lab. Moreover, if $\mathbf{p}$ lies below OZ_Λ, i.e. $\mathbf{p} = (p, \theta, \pi)$, then $\alpha = +\theta_{\text{Wick}}$ and $\mathcal{P}_T$ points in the opposite direction to the case $\mathbf{p} = (p, \theta, 0)$. Since, in addition, there is cylindrical symmetry about OZ_{L} we end up with a correlation between the position of the virtual source in the $X_{\text{L}}Y_{\text{L}}$-plane and the magnitude and direction of $\mathcal{P}_T$. This is shown qualitatively in Fig. 6.21.

The construction of these tertiary proton and antiproton beams was completed in 1989 and a major experimental programme was begun. Many of the asymmetries, e.g. in inclusive π^0 production, originally discovered at much lower energies, persist at higher energies, and a rich harvest of results has emerged. These are discussed in Chapter 13.

https://doi.org/10.1017/9781009402040.006 Published online by Cambridge University Press